Supplemental material for
Inverse 3D Microscopy Rendering for Cell Shape Inference with Active Mesh

Sacha Ichbiah Anshuman Sinha Fabrice Delbary Hervé Turlier
enter for Interdisciplinary Research in Biology, Collège de France
CNRS, Inserm, PSL University, Paris, France
herve.turlier@college-de-france.fr

1. Supplemental figures

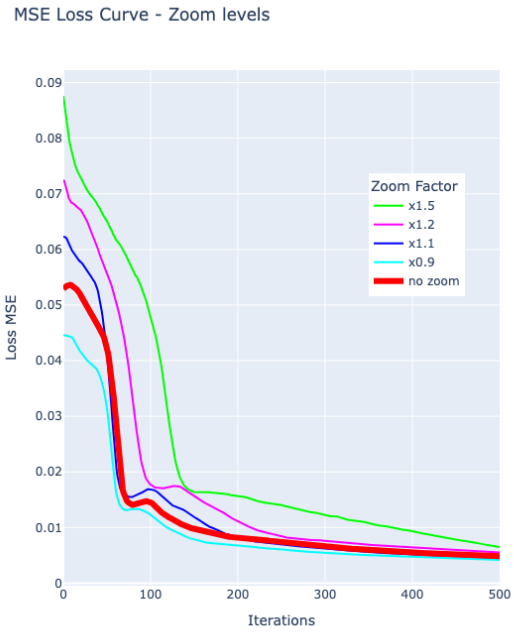

Supplemental figure 1: Plot of the loss function as function of the iteration number for the shape inference based on the mesh *Spot*, for several zoom factors applied to the initial mesh (from $\times 0.9$ to $\times 1.5$). Related to Figure 8.

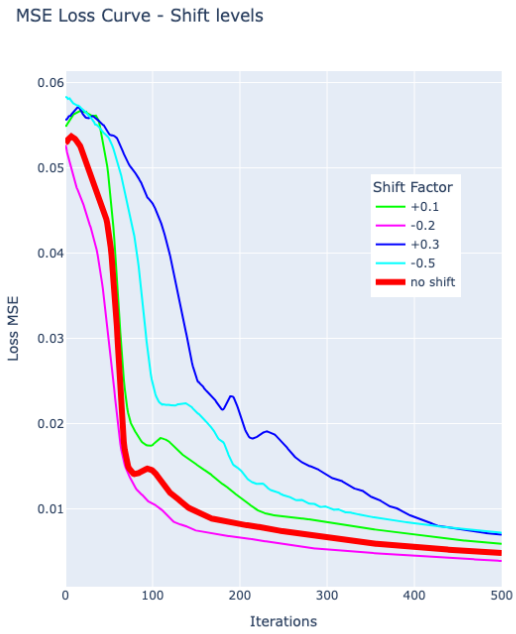

Supplemental figure 2: Plot of the loss function as function of the iteration number for the shape inference based on the mesh *Spot*, when a shift factor Δ/R is applied to the initial spherical mesh of radius R (from -0.5 to $+0.3$). Related to Figure 8.

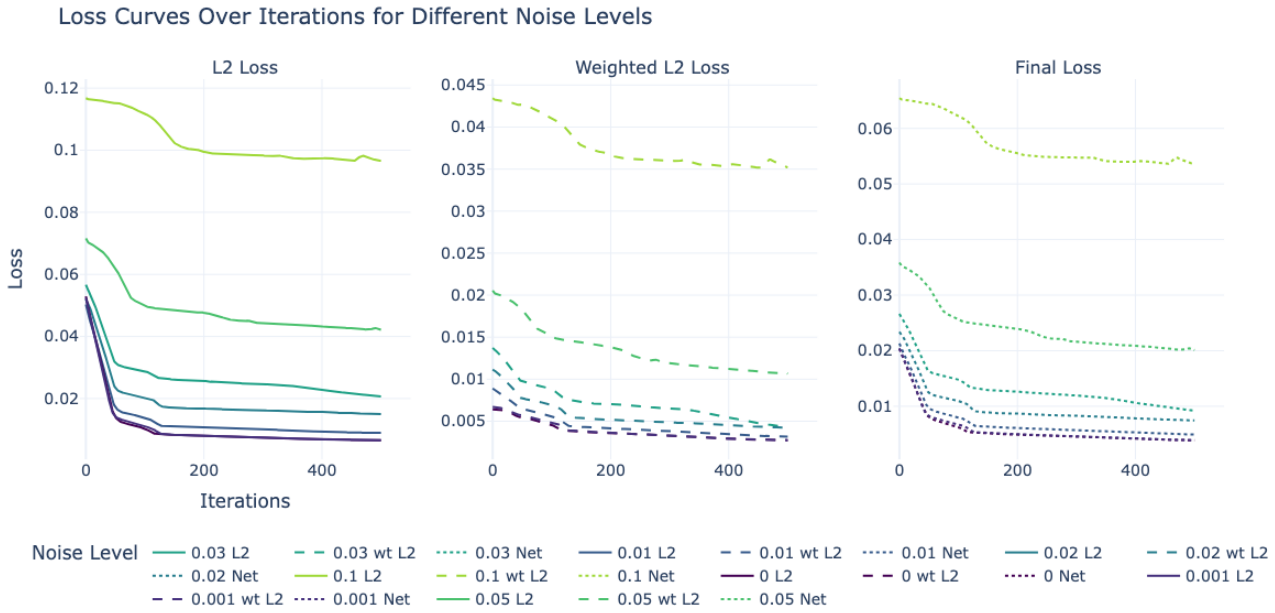

Supplemental figure 3: Loss functions (L2 loss, weighted L2 loss and net loss) as function of the iteration number for the shape inference based on the mesh *Spot*, when random noise is added to the target image (from 0.01 to 0.1). Related to Figure 8.

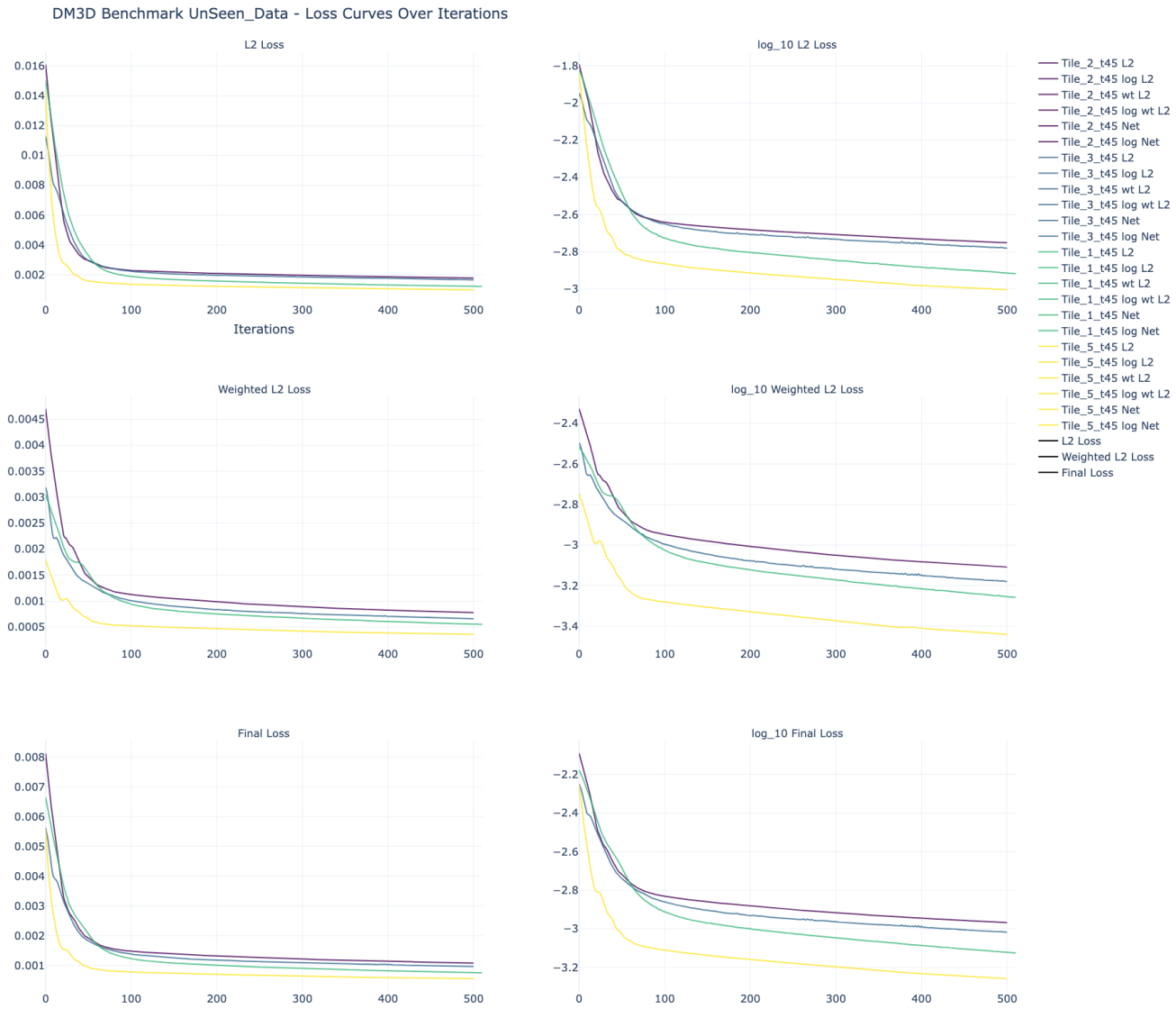

Supplemental figure 4: Representative plots of the Loss function logged as function of iterations for cellular shape inference from mouse organoid 3D fluorescence microscopy images. The 3 rows of plots (left: regular, right: logarithmic) represent the individual losses: MSE, weighted MSE and the final linearly-combined loss. These are the individual losses of running *deltaMic* per data item on benchmarked algorithm - DM3D's 'Unseen Dataset'. This dataset has been specifically chosen for benchmarking because although *deltaMic* is not a learning algorithm, **DM3D uses a CNN trained on the other datasets**. Related to Figure 9.

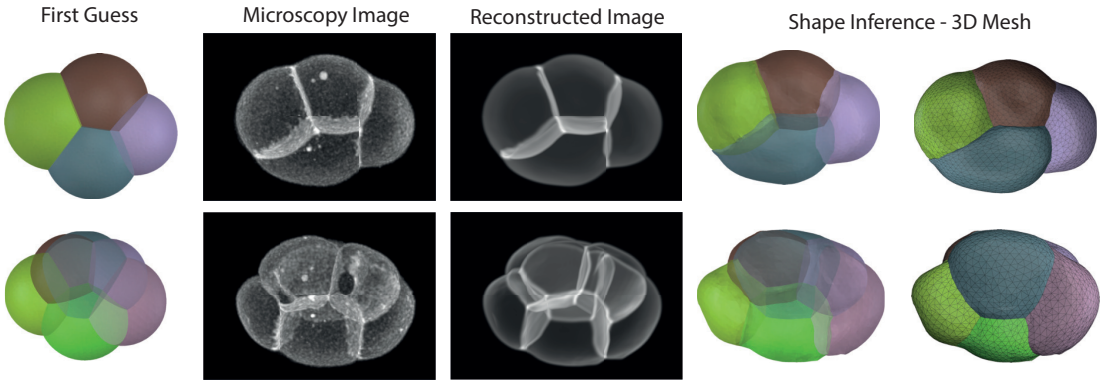

Supplemental figure 5: Cell shape inference in *C. elegans* embryos - 4 and 6 cell stages. See also: Supplemental videos 5-6. Extension of Figure 10.

2. Supplemental videos

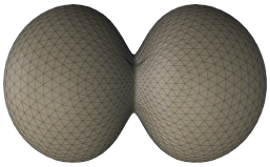

Supplemental video 1: Shape inference optimization process from a 3D artificial fluorescence microscopy image of a dividing cell. Related to Figure 7.

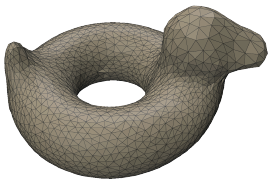

Supplemental video 2: Shape inference optimization process from a 3D artificial fluorescence microscopy image of the mesh *Bob*. Related to Figure 7.

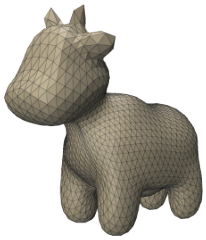

Supplemental video 3: Shape inference optimization process from a 3D artificial fluorescence microscopy image of the mesh *Spot*. Related to Figure 7.

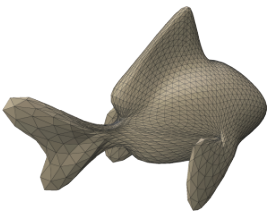

Supplemental video 4: Shape inference optimization process from a 3D artificial fluorescence microscopy image of the mesh *Blub*. Related to Figure 7.

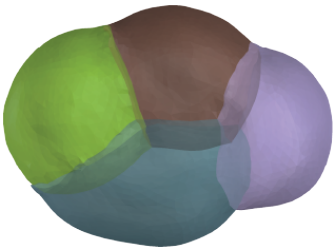

Supplemental video 5: Cell shape inference optimization process from a true confocal fluorescence microscopy image of a 4-cell stage *C. elegans* embryo. Supplemental Figure 5.

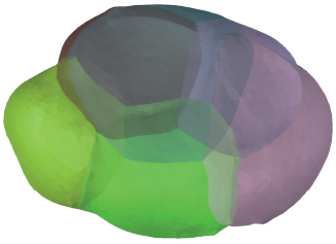

Supplemental video 6: Cell shape inference optimization process from a true confocal fluorescence microscopy image of a 6-cell stage *C. elegans* embryo. Related to Supplemental Figure 5.

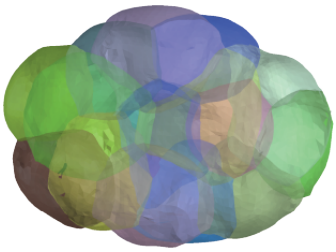

Supplemental video 7: Cell shape inference optimization process from a true confocal fluorescence microscopy image of a 16-cell stage *C. elegans* embryo. Related to Figure 10.

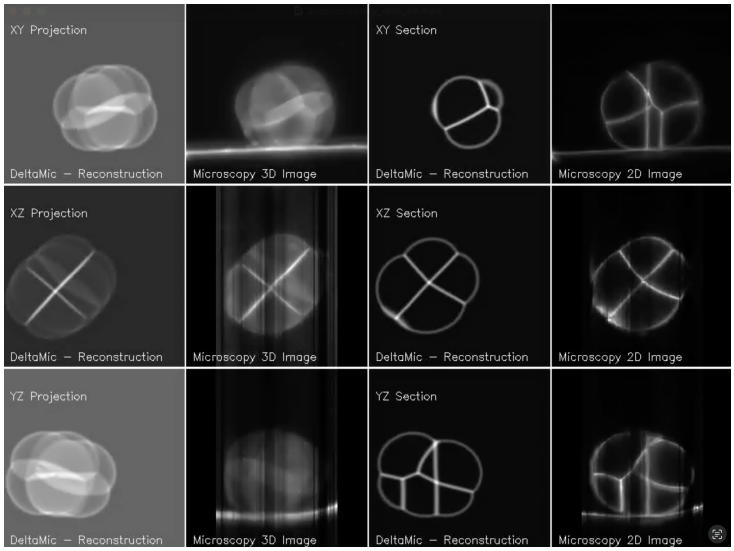

Supplemental video 8: Evolution of the cell shape inference optimization process from initial state to match the dual-view light-sheet fluorescence microscopy image of an 8-cell stage Ascidian embryo. Related to Figure 10.

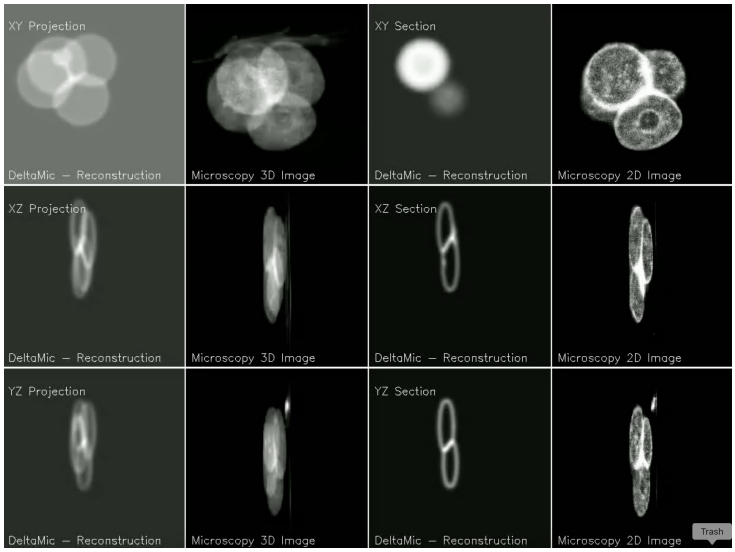

Supplemental video 9: Evolution of the cell shape inference optimization process from initial state to match the single-view light-sheet fluorescence microscopy image of a 4-cell stage Mouse embryo. Related to Figure 10.